Supplement of Atmos. Chem. Phys., 23, 551–563, 2023
https://doi.org/10.5194/acp-23-551-2023-supplement

Atmospheric Chemistry and Physics
Open Access
EGU

Supplement of

Quantifying daily NO_x and CO_2 emissions from Wuhan using satellite observations from TROPOMI and OCO-2

Qianqian Zhang et al.

Correspondence to: K. Folkert Boersma (folkert.boersma@wur.nl) and Qianqian Zhang (zhangqq@cma.gov.cn)

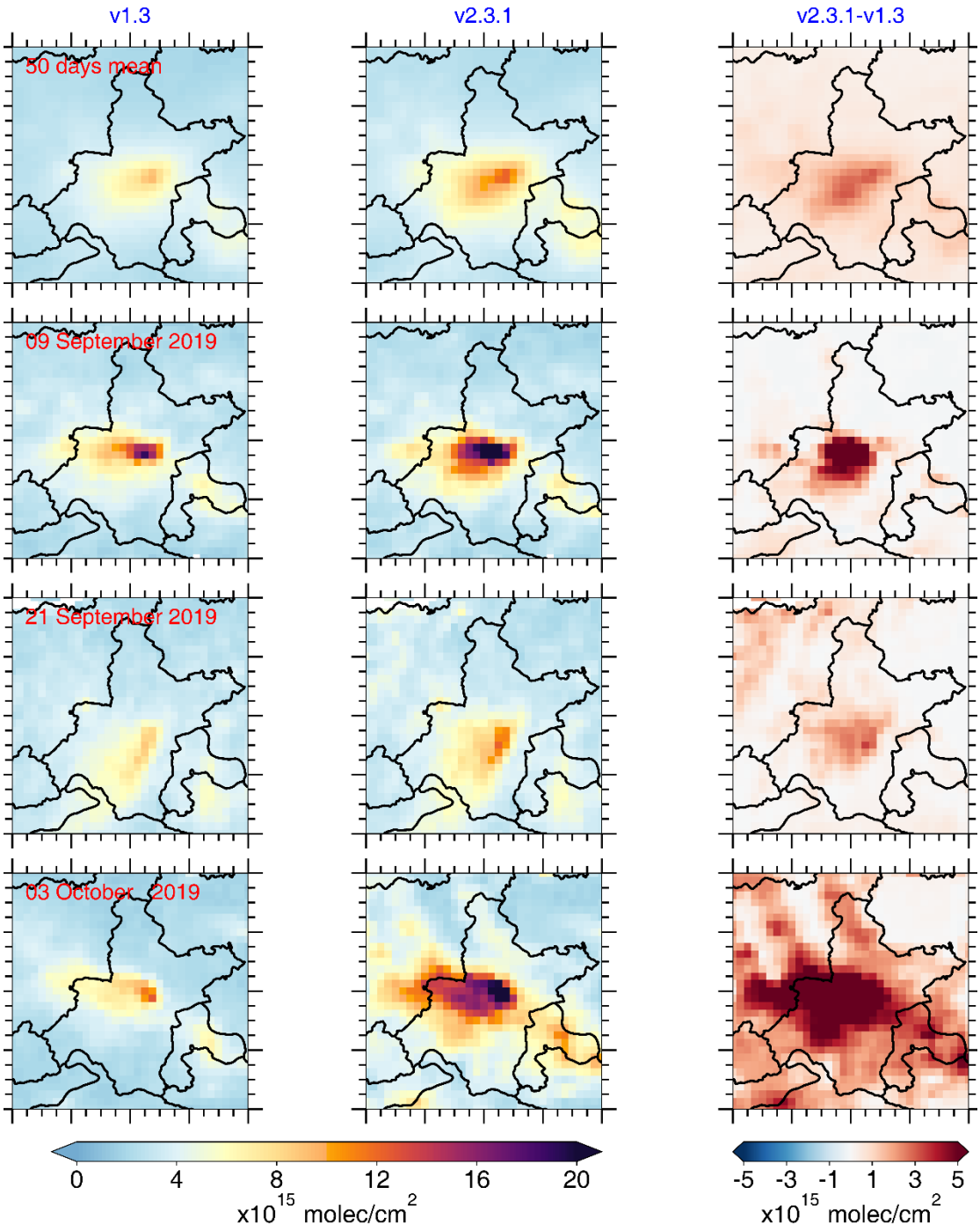

Figure S1: the difference in tropospheric NO_2 column densities between the version 2.3.1 and version 1.3 of TROPOMI data. From top to bottom: the 50 valid days mean in the study period, 09, 21 September, and 03 October 2019.

1. Emission spatial patterns

In the process of fitting the NO_x emissions from Wuhan, we give the first guess of the spatial pattern of NO_x emission, i.e., the spatial pattern from the MEIC-2017 and ABACAS-2019 bottom-up inventories (blue and black lines in Fig. S2). To be mentioned, the top-down NO_x emission pattern is smoother compared to the bottom-up emissions. The spatial pattern of the bottom-up emission inventories is used only as a first guess for the predicted emissions, we let it shift along with the wind during the fitting, and the final predicted NO_x emission pattern is determined by the mean of all the valid days.

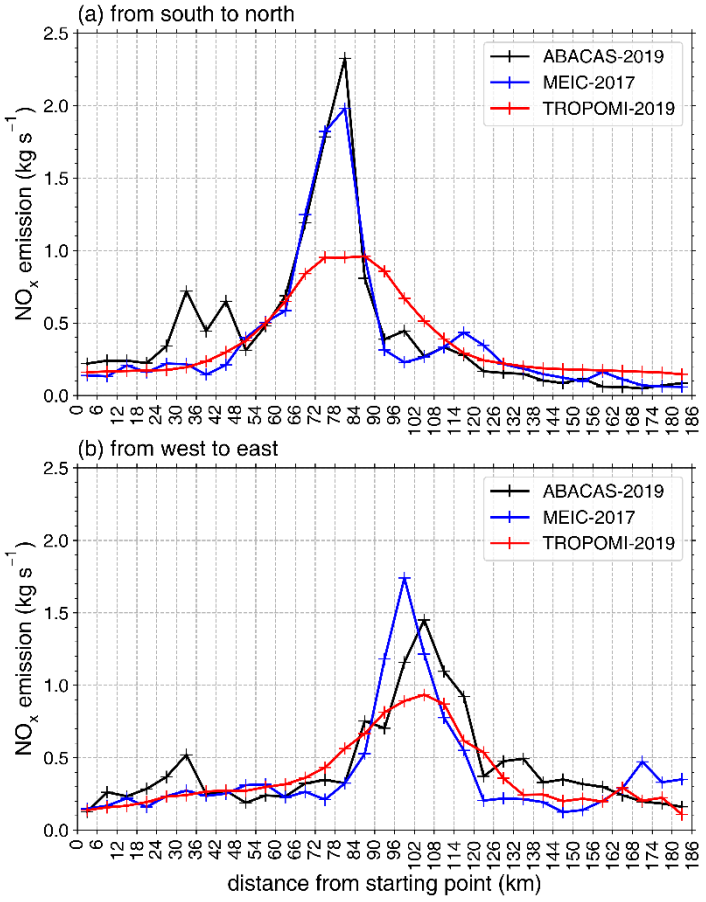

Figure S2: Spatial pattern of NO_x emissions in Wuhan from ABACAS-EI, MEIC, and our estimated results.

2. Data input into the model besides satellite data and bottom-up emissions

We use the 12.1 version of the GEOS-Chem model, with a horizontal resolution of 0.25° × 0.3125° (~ 30 × 37.5 km^2) to provide the a priori guesses for chemical parameters relevant to daytime NO_x. The satellite overpasses at around 13:30 local time, when NO_2 is mainly subject to first-order loss with reaction to the hydroxyl radical (OH). The loss rate for NO_x is expressed as $k = \frac{k' \times [OH]}{[NO_x]/[NO_2]}$, where k' is the first-order reaction rate constant (2.8×10^{-11} cm^3/molec/s according to the GEOS-Chem model), $[NO_x]/[NO_2]$ is the mean ratio between NO_x and NO_2 within the boundary layer. We calculated from GEOS-Chem the boundary layer mean NO_x/NO_2 ratio over Wuhan to be 1.26 from September 2019 to August 2020 over Wuhan, and used the annual mean value 1.26 in the fitting, and it is close to that used in Liu et al. (2016) (1.32).

The OH concentration is highly uncertain, and in-situ observations are sparse. In this study, we use the GEOS-Chem model simulated boundary layer mean OH concentration at 13:00 local time as our first guess and allow it to change by ±20% in the fitting procedure. In addition, OH simulations from the CMAQ model that has a higher spatial resolution are used as a reference. The fraction of boundary layer NO_2 columns of the tropospheric total is also from GEOS-Chem and places typically about 90% of tropospheric NO_2 columns within the boundary layer. Typically, in the daytime, NO_x are mainly subjected to photochemical reaction with the hydroxyl radical (OH) to produce nitric acid (HNO_3), which is quickly converted to nitrate aerosols (NO_3^-). In some rural regions with substantial VOCs emissions, NO_x may also react with VOCs: $CH_3O_2 + NO_2 + M <-> PAN + M$ (e. g., Fischer et al., 2014). We have compared the GEOS-Chem model simulated HNO_3+NO_3^- and PAN concentrations over our study domain in daytime:

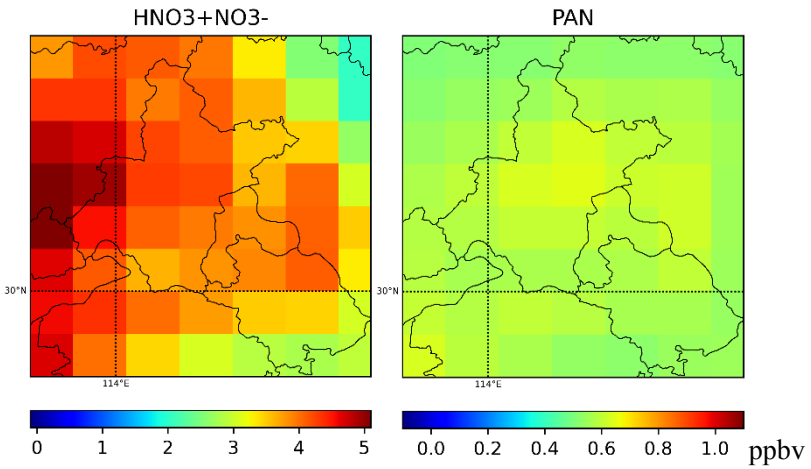

Figure S3: GEOS-chem model simulated monthly mean HNO3+NO3- (left) and PAN (right) concentration for July 2020.

The modeled HNO_3+NO_3^- concentration is 5–10 times higher than PAN over Wuhan, indicating that NO_x loss via OH is the driving pathway of NO_x chemistry over our study domain in the daytime.

At night, NO_2 is oxidized to HNO_3 through the formation of N_2O_5 and NO_3 and heterogeneous reactions, including water vapor and aerosols (Shah et al., 2020; Lamsal et al., 2010). The overpass time of the satellite is 13:00–13:30 local time when NO_x chemistry over the city is dominated by the photochemical process, so we consider the reaction between NO_x and OH in the superposition column model as the main loss pathway.

Boundary layer mean wind fields are from ERA5, the fifth generation ECMWF atmospheric reanalysis of the global climate (Hersbach et al., 2020). We use the 05:00 UTC time (13:00 Wuhan time) zonal and meridional winds, with a horizontal resolution of 0.25 ° × 0.25 °. Mean wind speed within the boundary layer is calculated using the average of the wind speeds at all vertical layers within the boundary layer weighted by the NO_2 columns within each vertical layer.

3. NO_2 line density

This part demonstrates the way to achieve the 1-D distribution of satellite observed NO_2 along wind direction. First, we define the study domain, the red circle in Fig. S4, including the whole area of Wuhan, as well as other small cities around Wuhan (the blue circle is the Third Ring Road of Wuhan, ~50% of

NO_x emissions in the red circle are within the blue circle). Then, we resample the TROPOMI NO_2 data at 6km×6km spatial resolution and rotate it toward the wind direction. For our study domain, we get 31×31 grid cells. Second, we divide the 31×31 grid cells into 31 'line cells' along the wind direction, as shown with the pink grids in Fig. S4. Each cell is 186km wide (perpendicular to wind direction) and 6km long (along wind direction). Third, the NO_2 line density (mole cm^{-1}) within each line cell is calculated by accumulating NO_2 column density (mole cm^{-2}) of all the 31 grid cells within the line cell, and then we obtain the NO_2 line density along wind direction as shown in the right panel of Fig. S4.

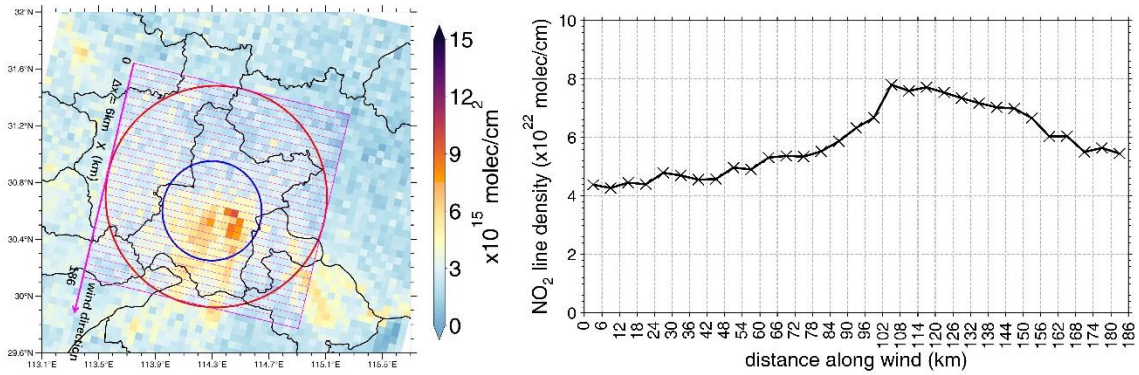

Figure S4. Left panel: tropospheric NO_2 column on 18 May 2020. The data is sampled with 0.05° (longitude) × 0.05° (latitude) grid size (~6×6km^2) and rotated toward the wind direction. The red circle centered at 114.3°E, 30.7°N represents our study domain, with a diameter of ~186km (31 cells along wind and 31 cells perpendicular to the wind), and the blue circle defines the area within the Third Ring Road of Wuhan. For each cell along the wind, 31 cells perpendicular to the wind are accumulated to make up the line density of NO_2 (right panel).

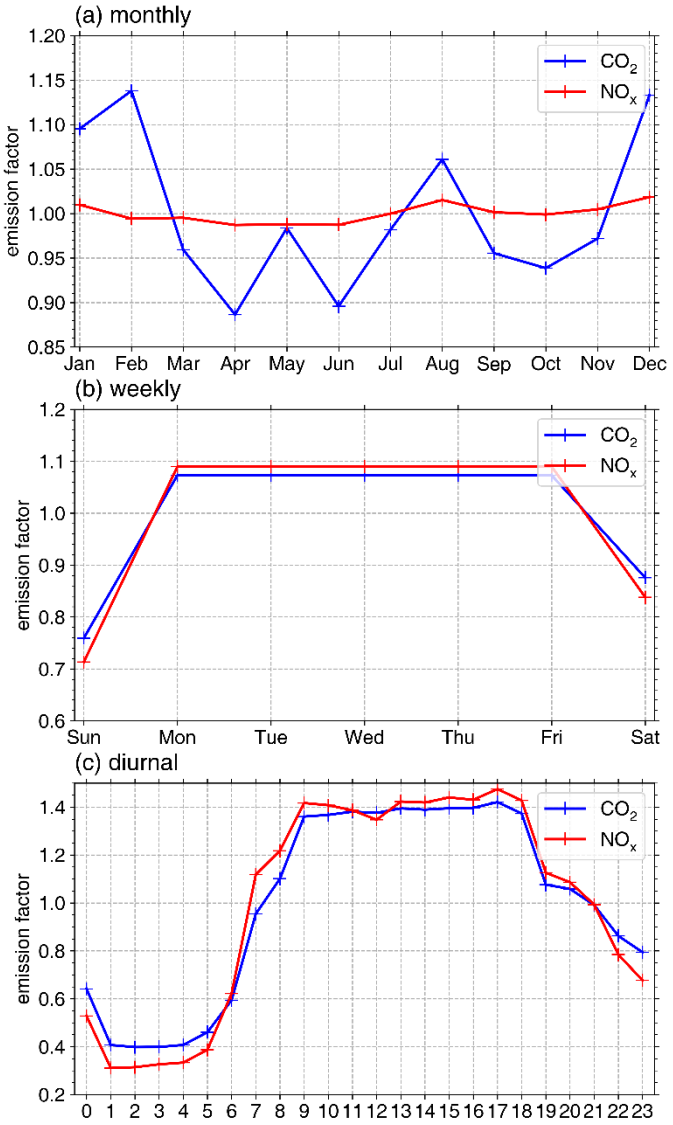

Figure S5. The (a) monthly, (b) weekly and (c) diurnal variation of NO_x and CO_2 emissions from Wuhan. The time factor is provided by ABACAS-EI, MEIC and GEOS-Chem model.

4. Robustness with respect to the area of study domain

We chose a relatively large area as our study domain (a circular region centered at 114°E, 30.7°N, with a diameter of ~186km, Fig. S6 left panel, red circle.) to ensure the whole area of Wuhan is included. However, according to the bottom-up emission inventories (Fig. S2), more than 50% of the NO_x emissions in this area are concentrated within the Third Ring Road of Wuhan (84 km diameter, Fig. S6 the blue circle in the left panel). The large study domain (186km wide of each cell along the NO_2 line density) may smear off the build-up of NO_2 in the high-emission area and thus impact the estimated NO_x lifetime and emissions. To verify the robustness of our model to the area of the study domain, we randomly choose 3 days (8 September 2019, 10 November 2019, and 7 March 2020), and narrow down the study domain to the blue circle in Fig. S6. In Fig. S6 we compare NO_x lifetimes and emissions from the inside of the Third Ring Road of Wuhan between the two situations with different area sizes of the study domain. Notably, the NO_2 column density within this smaller domain is higher than outside. The OH radical is the major oxidizing agent to convert primary pollutants to secondary ones in the atmosphere, so the concentration of OH radical concentration is lower inside (Tan et al., 2018). Consequently, the lifetime of NO_x inside the smaller domain will be longer.

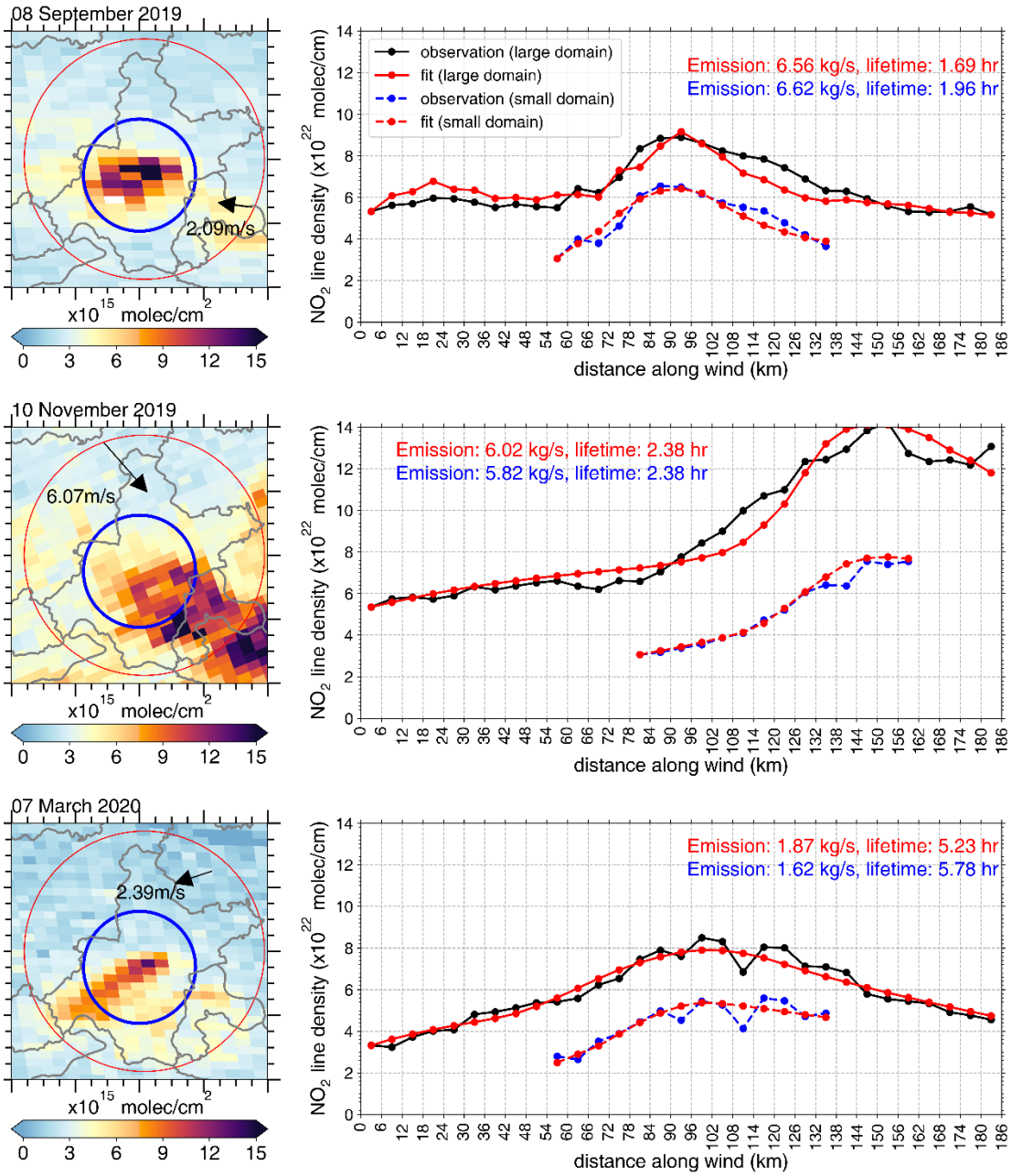

Figure S6. A comparison of NO_x emissions and lifetimes inside the Third Ring Road of Wuhan (blue circles in the left panel) using the superposition model under the two situations with large (red circles in the left panel) and small (blue circles in the left panel) study domains. NO_x emissions and lifetimes within the Third Ring Road of Wuhan are listed in the right panel.

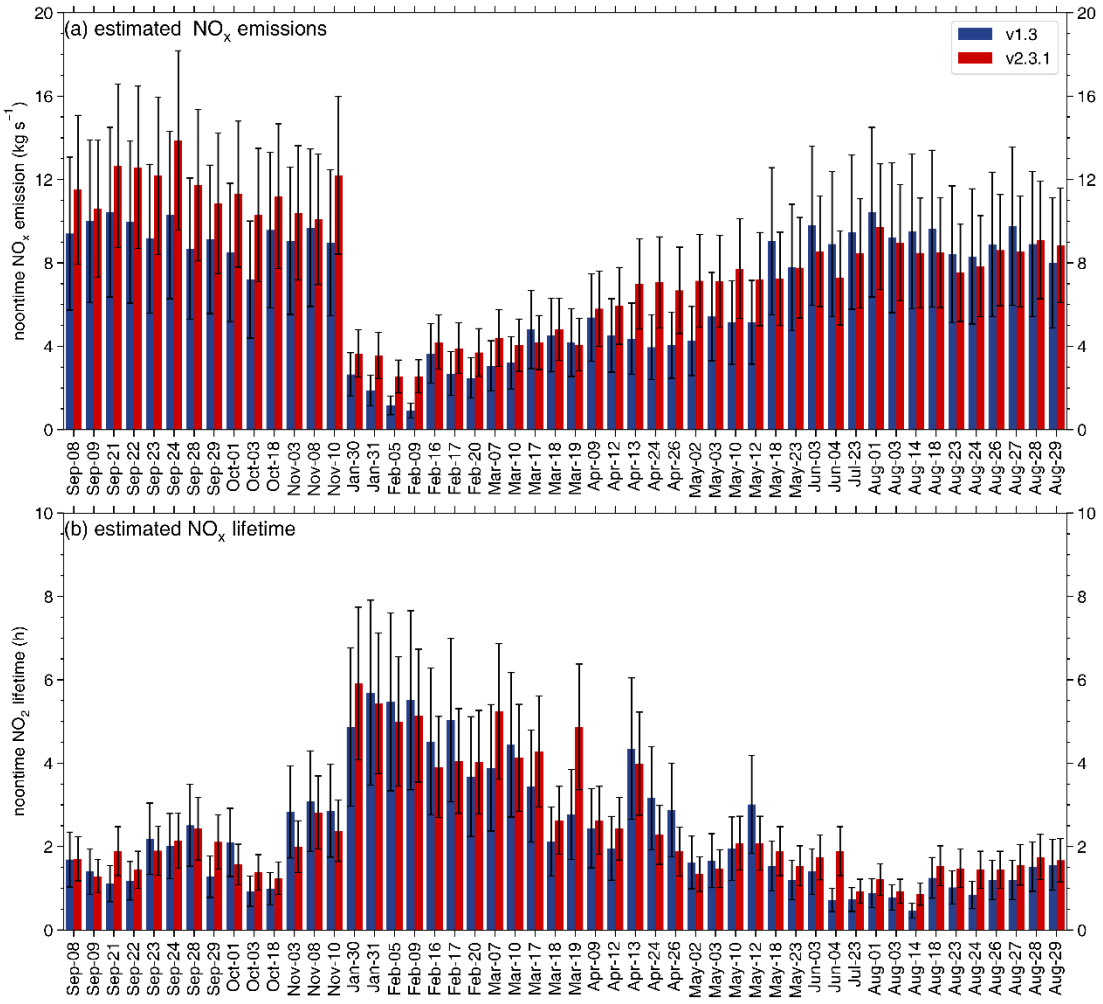

Figure S7. Estimated NO_x (a) emissions and (b) lifetime over Wuhan during the study period based on the TROPOMI-v1.3 (blue bars) and TROPOMI-v2.3.1 (red bars) datasets. The error bars denote the corresponding uncertainty.

5. The Gaussian plume model

To compare with the results from our superposition column model, we further use a Gaussian plume model (Bovensmann et al., 2010; Zheng et al., 2020) to estimate the XCO_2 enhancement due to Wuhan CO_2 emissions. XCO_2 enhancement on each point of the satellite orbit is contributed from the sum of all CO_2 emissions on the upwind region of the orbit:

$$C_{CO_2} = \sum \frac{E_{CO_2}}{\sqrt{2\pi} \times a \times u \times x^{0.894}} \times EXP[-\frac{1}{2}\left(\frac{y}{a \times x^{0.894}}\right)^2] \quad (1)$$

$$XCO_2 = C_{CO_2} \times \frac{M_{air}}{M_{CO_2}} \times \frac{g}{P_{surf} - w \times g} \times 10^3 \quad (2)$$

In Eq. (1), E_{CO_2} denotes the top-down CO_2 emission (g/s) and C_{CO_2} is the CO_2 column concentration enhancement (g/m^2) relative to the background. u is wind speed in m/s, x (km) and y (m) are the along wind and across wind distance from the location of the point emission source, respectively. a is the atmospheric stability parameter and the value is taken following Masters and Ela (2007). Eq. (2) is performed to convert C_{CO_2} to XCO_2, in which M_{air} and M_{CO_2} are the molecular weight of air and CO_2, g is the gravitational acceleration 9.8m/s^2. P_{surf} is the surface pressure (Pa) and w is the total column water content (kg/m^2), both of which can be accessed from the second Orbiting Carbon Observatory (OCO-2) satellite data file.

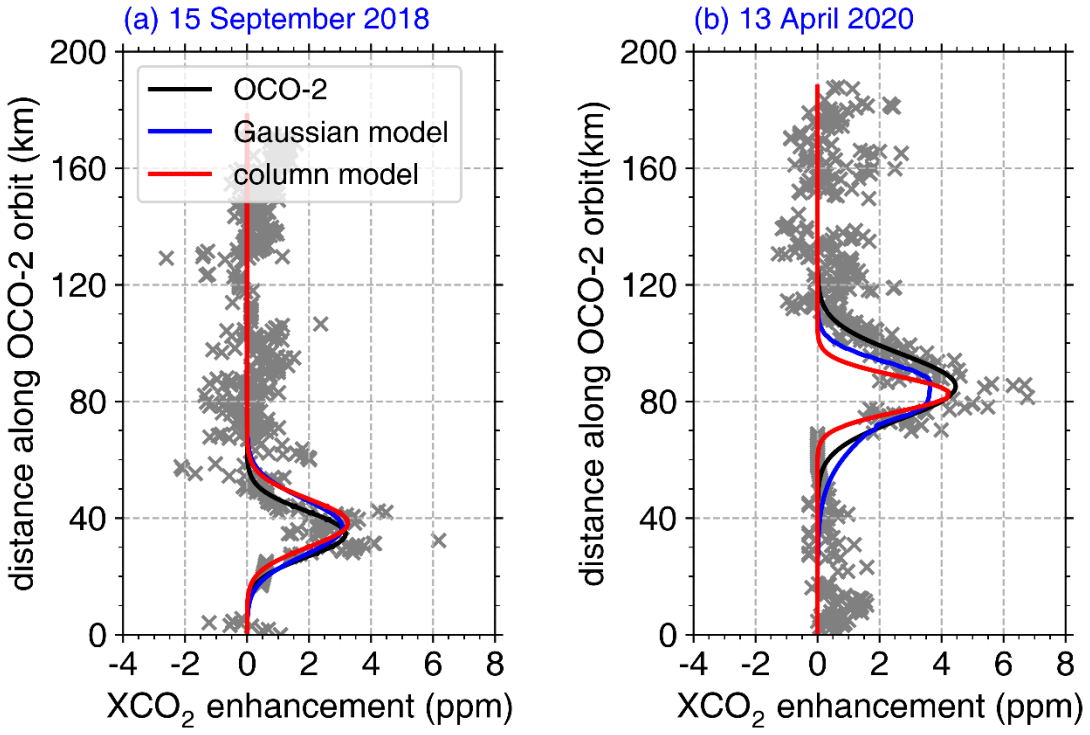

Figure S8. XCO_2 enhancement observations from OCO-2 (gray dots and black lines), and estimation with our top-down CO_2 emissions from the Gaussian plume model (blue lines) and the superposition model (red lines) on (a) 15 September 2018 and (b) 13 April 2020.

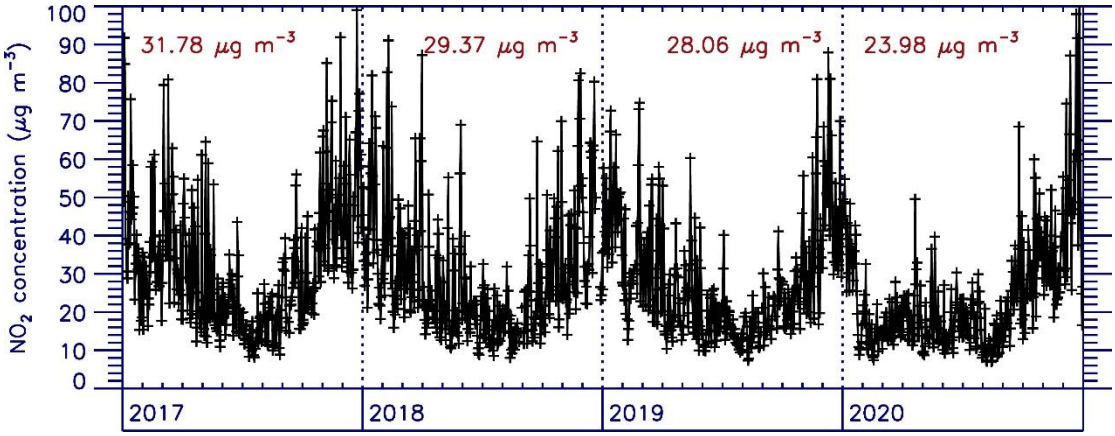

Figure S9. Daily noontime (13:00 and 14:00 mean) surface observed NO_2 concentration from 2017 to 2020. The annual mean concentration for each year is listed. The data is from the China National Environmental Monitoring Center (CNEMC) network, including 11 sites in Wuhan.

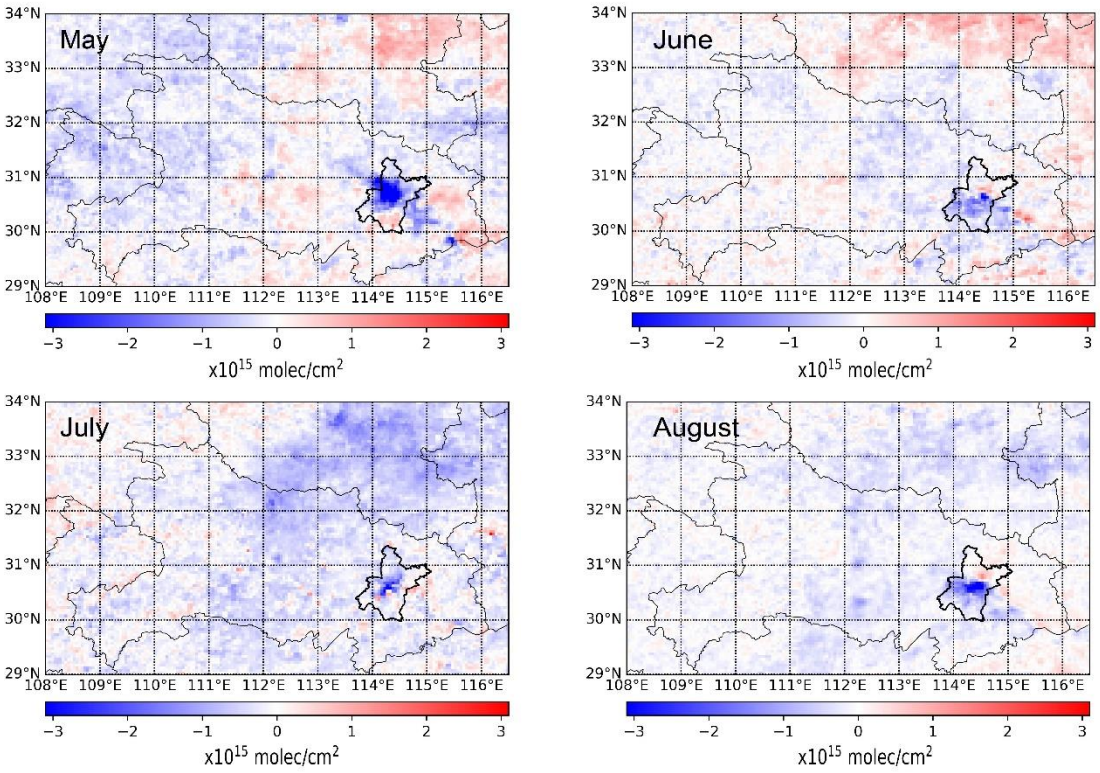

Figure S10. The difference in monthly mean NO_2 column between 2020 and 2019 (2020 minus 2019) over Hubei Province.

Table S1. NO_x and CO_2 emissions over Wuhan inferred from TROPOMI and related information of 50 days from September 2019 to August 2020.

day		NO_x emission (kg/s)	NO_x lifetime (hrs)	CO_2-to-NO_x Emission ratio (g CO_2/g NO_x)	CO_2 emission (kt/s)	wind speed (m/s)	wind direction (°)	back_offset $\times 10^{22}$ molec/cm	back_slope ($\times 10^{-22}$ molec/cm^2)	surface temperature (℃)	PBL height (m)	initial GC OH concentration (molec/cm^3)	initial CMAQ OH concentration (molec/cm^3)	OH concentration best fit (molec/cm^3)	R
2019/9/8	Tue	11.51±3.57	1.71±0.53	533±159.9	6.13±3.00	2.1	59 (ENE)	4.89E+22	-0.002	35	1274	7.63E+06	1.51E+07	7.31E+06	0.91
2019/9/9	Wed	10.6±3.29	1.29±0.4	533±159.9	5.65±2.77	2.64	111 (ESE)	4.42E+22	0.001	35	1321	8.17E+06	1.50E+07	9.69E+06	0.96
2019/9/21	Mon	12.65±3.92	1.89±0.59	533±159.9	6.74±3.30	10.6	22 (NNE)	4.73E+22	-0.004	27	1652	7.29E+06	1.37E+07	6.61E+06	0.92
2019/9/22	Tue	12.58±3.9	1.44±0.45	533±159.9	6.7±3.28	9.92	29 (NNE)	6.11E+22	-0.01	28	1569	7.97E+06	1.24E+07	8.68E+06	0.95
2019/9/23	Wed	12.18±3.78	1.9±0.59	533±159.9	6.49±3.18	6.42	22 (NNE)	3.87E+22	0.005	30	1869	8.35E+06	1.21E+07	6.58E+06	0.97

2019/9/24	Thu	13.88±4.3	2.14±0.66	533±159.9	7.4±3.63	2.96	40 (NE)	4.96E+22	0.01	30	960	7.29E+06	1.22E+07	5.84E+06	0.96
2019/9/28	Sat	11.73±3.64	2.43±0.75	566±169.8	6.63±3.25	2.34	28 (NNE)	5.25E+22	-0.001	32	929	5.97E+06	1.18E+07	5.14E+06	0.98
2019/9/29	Sun (work)	10.86±3.37	2.11±0.65	533±159.9	5.79±2.84	2.54	88 E	6.87E+22	-0.002	33	1071	5.95E+06	1.12E+07	5.92E+06	0.92
2019/10/1	Tue (holiday)	11.3±3.5	1.57±0.49	533±159.9	6.02±2.95	3.29	23 (NNE)	4.32E+22	0	34	862	8.23E+06	1.03E+07	7.96E+06	0.98
2019/10/3	Thu (holiday)	10.3±3.19	1.38±0.43	533±159.9	5.48±2.69	1.52	175 (S)	6.11E+22	-0.005	32	1203	8.86E+06	1.03E+07	9.06E+06	0.96
2019/10/18	Fri	11.2±3.47	1.24±0.38	550±165	6.16±3.02	2.94	325 (NW)	4.27E+22	-0.002	27	1343	8.61E+06	6.99E+06	1.01E+07	0.96
2019/11/3	Sun	10.4±3.22	2±0.62	604±181.2	6.29±3.08	6.25	359 (N)	5.43E+22	0	26	1231	7.44E+06	6.10E+06	6.25E+06	0.97

2019/11/8	Fri	10.09±3.13	2.82±0.87	559±167.7	5.64±2.76	1.2	53 (NE)	2.74E+22	0	24	1539	5.52E+06	5.46E+06	4.43E+06	0.87
2019/11/10	Sun	12.2±3.78	2.38±0.74	604±181.2	7.37±3.61	6.07	320 (NW)	5.10E+22	-0.001	25	1270	3.59E+06	6.49E+06	5.25E+06	0.97
2020/1/30	Thu (lockdown)	3.65±1.13	5.91±1.83	716±214.8	2.61±1.28	2.16	343 (NNW)	4.80E+22	-0.02	15	1066	9.77E+05	1.22E+06	2.12E+06	0.96
2020/1/31	Fri (lockdown)	3.56±1.1	5.44±1.69	716±214.8	2.55±1.25	2.92	155 (SSE)	5.13E+22	-0.01	14	794	1.91E+06	1.81E+06	2.30E+06	0.85
2020/2/5	Wed (lockdown)	2.55±0.79	5±1.55	674±202.2	1.72±0.84	4.93	105 (ESE)	3.67E+22	0	15	870	3.13E+06	3.14E+06	2.50E+06	0.85
2020/2/9	Sun (lockdown)	2.56±0.79	5.14±1.59	729±218.7	1.86±0.91	1.44	272 (W)	4.05E+22	-0.005	15	851	3.10E+06	3.30E+06	2.43E+06	0.9

2020/2/16	Sun (lockdown)	4.2±1.3	3.91±1.21	729±218.7	3.06±1.50	5.97	336 (NNW)	1.64E+22	-0.01	7	1365	3.34E+06	3.36E+06	3.20E+06	0.96
2020/2/17	Mon (lockdown)	3.91±1.21	4.05±1.26	674±202.2	2.64±1.29	4.56	342 (NNW)	3.32E+22	-0.002	13	1358	3.67E+06	3.45E+06	3.09E+06	0.95
2020/2/20	Thu (lockdown)	3.7±1.15	4.02±1.25	674±202.2	2.49±1.22	4.52	124 (SE)	3.48E+22	-0.015	17	956	3.72E+06	4.64E+06	3.11E+06	0.9
2020/3/7	Sat (lockdown)	4.39±1.36	5.24±1.62	663±198.9	2.91±1.43	2.39	72 (ENE)	2.94E+22	-0.02	19	660	2.63E+06	4.73E+06	2.39E+06	0.97
2020/3/10	Tue (lockdown)	4.05±1.26	4.13±1.28	625±187.5	2.53±1.24	4.94	336 (NNW)	3.00E+22	-0.02	18	1173	2.33E+06	6.69E+06	3.03E+06	0.98

2020/3/17	Tue (lockdown)	4.18±1.3	4.28±1.33	625±187.5	2.61±1.28	3.39	273 (W)	2.43E+22	0	21	1356	3.49E+06	7.41E+06	2.92E+06	0.94
2020/3/18	Wed (lockdown)	4.81±1.49	2.63±0.82	625±187.5	3.00±1.47	5.2	225 (SW)	3.43E+22	-0.01	23	1046	4.37E+06	8.11E+06	4.75E+06	0.92
2020/3/19	Thu (lockdown)	4.08±1.26	4.87±1.51	625±187.5	2.55±1.25	3.2	36 (NE)	3.63E+22	-0.015	23	1057	3.60E+06	8.66E+06	2.57E+06	0.96
2020/4/9	Thu	5.8±1.8	2.63±0.82	635±190.5	3.68±1.8	3.4	179 (S)	5.06E+22	-0.01	27	1465	4.51E+06	9.69E+06	4.75E+06	0.95
2020/4/12	Sun	5.94±1.84	2.43±0.75	674±202.2	4.00±1.96	7.43	311 (NW)	4.59E+22	0	21	1948	5.60E+06	1.03E+07	5.14E+06	0.97
2020/4/13	Mon	6.99±2.17	3.99±1.24	635±190.5	4.44±2.18	1.67	272 (W)	5.43E+22	-0.01	22	1719	4.93E+06	9.41E+06	3.13E+06	0.96
2020/4/24	Fri	7.06±2.19	2.28±0.71	635±190.5	4.48±2.2	5.39	264 (W)	2.16E+22	0	22	2427	6.58E+06	1.16E+07	5.48E+06	0.92

2020/4/26	Sun (work)	6.68±2.07	1.88±0.58	635±190.5	4.24±2.08	5.49	242 (WSW)	3.89E+22	0.001	27	1282	6.45E+06	1.36E+07	6.65E+06	0.89
2020/5/2	Sat (holiday)	7.14±2.21	1.34±0.42	628±188.4	4.48±2.20	6.49	238 (WSW)	4.73E+22	-0.01	26	944	8.02E+06	1.75E+07	9.33E+06	0.91
2020/5/3	Sun (holiday)	7.12±2.21	1.47±0.46	640±192	4.55±2.23	4.35	198 (SSW)	4.10E+22	-0.005	27	1312	7.80E+06	1.85E+07	8.50E+06	0.97
2020/5/10	Sun	7.72±2.39	2.08±0.64	640±192	4.94±2.42	3.42	324 (NW)	1.44E+22	0.002	27	1370	7.51E+06	1.48E+07	6.01E+06	0.97
2020/5/12	Tue	7.22±2.24	2.08±0.64	592±177.6	4.27±2.09	4.1	297 (WNW)	1.56E+22	-0.005	30	1693	5.93E+06	1.41E+07	6.01E+06	0.89
2020/5/18	Mon	7.23±2.24	1.89±0.59	592±177.6	4.28±2.10	6.91	8 (N)	4.26E+22	-0.005	36	1546	7.55E+06	1.61E+07	6.61E+06	0.96
2020/5/23	Sat	7.77±2.41	1.54±0.48	628±188.4	4.88±2.39	3.51	197 (SSW)	4.01E+22	-0.01	35	1521	8.36E+06	1.78E+07	8.12E+06	0.96

2020/6/3	Wed	8.56±2.65	1.74±0.54	530±159	4.54±2.22	2.29	107 (ESE)	3.67E+22	0	31	969	9.22E+06	1.16E+07	7.18E+06	0.96
2020/6/4	Thu	7.28±2.26	1.89±0.59	530±159	3.86±1.89	4.54	215 (SW)	2.05E+22	-0.01	33	1350	9.95E+06	1.50E+07	6.61E+06	0.95
2020/7/23	Thu	8.45±2.62	0.93±0.29	518±155.4	4.38±2.15	4.99	240 (WSW)	2.49E+22	-0.005	34	1040	1.23E+07	1.82E+07	1.34E+07	0.87
2020/8/1	Sat	9.73±3.02	1.21±0.38	619±185.7	6.02±2.95	4.34	205 (SSW)	3.62E+22	-0.02	34	977	1.02E+07	2.06E+07	1.03E+07	0.93
2020/8/3	Mon	8.97±2.78	0.93±0.29	583±174.9	5.23±2.56	4.4	201 (SSW)	2.96E+22	-0.02	37	1104	1.15E+07	2.14E+07	1.34E+07	0.94
2020/8/14	Fri	8.48±2.63	0.86±0.27	583±174.9	4.94±2.42	8.38	213 (SSW)	2.52E+22	-0.02	36	961	9.74E+06	2.03E+07	1.45E+07	0.93
2020/8/18	Tue	8.49±2.63	1.54±0.48	583±174.9	4.95±2.43	2.97	191 (S)	3.55E+22	-0.005	35	1151	7.17E+06	2.04E+07	8.12E+06	0.95
2020/8/23	Sun	7.52±2.33	1.48±0.46	630±189	4.74±2.32	3.86	193 (SSW)	3.01E+22	-0.02	32	941	5.62E+06	1.69E+07	8.45E+06	0.93

2020/8/24	Mon	7.84±2.43	1.44±0.45	583±174.9	4.57±2.24	6.87	241 (WSW)	2.75E+22	-0.02	34	1020	7.68E+06	1.88E+07	8.68E+06	0.91
2020/8/26	Wed	8.61±2.67	1.44±0.45	583±174.9	5.02±2.46	5.19	340 (NNW)	3.08E+22	0	31	1039	1.08E+07	1.55E+07	8.68E+06	0.96
2020/8/27	Thu	8.55±2.65	1.56±0.48	583±174.9	4.98±2.44	2.52	42 (NE)	3.48E+22	0	33	841	9.59E+06	1.45E+07	8.01E+06	0.95
2020/8/28	Fri	9.1±2.82	1.75±0.54	583±174.9	5.30±2.6	2.37	46 (NE)	3.81E+22	0	33	1089	8.54E+06	1.71E+07	7.14E+06	0.93
2020/8/29	Sat	8.85±2.74	1.67±0.52	619±185.7	5.47±2.68	4.39	36 (NE)	3.13E+22	0	33	1028	7.39E+06	1.72E+07	7.49E+06	0.94

Table S2. Uncertainty of each factors and their influence on NO_x and CO_2 emission estimation..

factor	uncertainty	Influence on NO_x and (or) CO_2 emissions
Satellite NO_2 retrieval	±20 %	20 %
OH concentration	±20 %	3 %
NO_2/NO_x ratio	±10 %	8 %
Wind field	±20 %	17 %
Area of study domain	/	15 %
CO_2-to-NO_x emission ratio	±30 %	30 %

References

Bovensmann, H., Buchwitz, M., Burrows, J. P., Reuter, M., Krings, T., Gerilowski, K., Schneising, O., Heymann, J., Tretner, A., and Erzinger, J.: A remote sensing technique for global monitoring of power plant CO_2 emissions from space and related applications, Atmos. Meas. Tech., 3, 781-811, 10.5194/amt-3-781-2010, 2010.

Fischer, E. V., Jacob, D. J., Yantosca, R. M., Sulprizio, M. P., Millet, D. B., Mao, J., Paulot, F., Singh, H. B., Roiger, A., Ries, L., Talbot, R. W., Dzepina, K., and Pandey Deolal, S.: Atmospheric peroxyacetyl nitrate (PAN): a global budget and source attribution, Atmos. Chem. Phys., 14, 2679-2698, 10.5194/acp-14-2679-2014, 2014.

Hersbach, H., Bell, B., Berrisford, P., Hirahara, S., Horányi, A., Muñoz‐Sabater, J., Nicolas, J., Peubey, C., Radu, R., Schepers, D., Simmons, A., Soci, C., Abdalla, S., Abellan, X., Balsamo, G., Bechtold, P., Biavati, G., Bidlot, J., Bonavita, M., Chiara, G., Dahlgren, P., Dee, D., Diamantakis, M., Dragani, R., Flemming, J., Forbes, R., Fuentes, M., Geer, A., Haimberger, L., Healy, S., Hogan, R. J., Hólm, E., Janisková, M., Keeley, S., Laloyaux, P., Lopez, P., Lupu, C., Radnoti, G., Rosnay, P., Rozum, I., Vamborg, F., Villaume, S., and Thépaut, J. N.: The ERA5 global reanalysis, Q J R Meteorol Soc., 146, 1999-2049, 10.1002/qj.3803, 2020.

Lamsal, L. N., Martin, R. V., van Donkelaar, A., Celarier, E. A., Bucsela, E. J., Boersma, K. F., Dirksen, R., Luo, C., and Wang, Y.: Indirect validation of tropospheric nitrogen dioxide retrieved from the OMI satellite instrument: Insight into the seasonal variation of nitrogen oxides at northern midlatitudes, J. Geophys. Res., 115, 10.1029/2009jd013351, 2010.

Liu, F., Beirle, S., Zhang, Q., Dörner, S., He, K., and Wagner, T.: NO_x lifetimes and emissions of cities and power plants in polluted background estimated by satellite observations, Atmos. Chem. Phys., 16, 5283-5298, 10.5194/acp-16-5283-2016, 2016.

Masters, G. M. and Ela, W. P.: Introduction to environmental engineering and science, Pearson, 3rd edition pp. 457, 2007.

Shah, V., Jacob, D. J., Li, K., Silvern, R. F., Zhai, S., Liu, M., Lin, J., and Zhang, Q.: Effect of changing

NO_x lifetime on the seasonality and long-term trends of satellite-observed tropospheric NO_2 columns over China, Atmos. Chem. and Phys., 20, 1483-1495, 10.5194/acp-20-1483-2020, 2020.

Tan, Z., Rohrer, F., Lu, K., Ma, X., Bohn, B., Broch, S., Dong, H., Fuchs, H., Gkatzelis, G. I., Hofzumahaus, A., Holland, F., Li, X., Liu, Y., Liu, Y., Novelli, A., Shao, M., Wang, H., Wu, Y., Zeng, L., Hu, M., Kiendler-Scharr, A., Wahner, A., and Zhang, Y.: Wintertime photochemistry in Beijing: observations of RO_x radical concentrations in the North China Plain during the BEST-ONE campaign, Atmospheric Chemistry and Physics, 18, 12391-12411, 10.5194/acp-18-12391-2018, 2018.

Zheng, B., Chevallier, F., Ciais, P., Broquet, G., Wang, Y., Lian, J., and Zhao, Y.: Observing carbon dioxide emissions over China's cities and industrial areas with the Orbiting Carbon Observatory-2, Atmos. Chem. Phys., 20, 8501-8510, 10.5194/acp-20-8501-2020, 2020.